Radiology

ORIGINAL RESEARCH • MUSCULOSKELETAL IMAGING

Virtual Noncalcium Dual-Energy CT: Detection of Lumbar Disk Herniation in Comparison with Standard Grayscale CT

Christian Booz, MD • Jochen Nöske, MED • Simon S. Martin, MD • Moritz H. Albrecht, MD • Ibrahim Yel, MD • Lukas Lenga, MD • Tatjana Gruber-Rouh, MD • Katrin Eichler, MD • Tommaso D'Angelo, MD • Thomas J. Vogl, MD • Julian L. Wichmann, MD

From the Division of Experimental and Translational Imaging (C.B., J.N., S.S.M., M.H.A., I.Y., L.L., T.D., J.L.W.) and Department of Diagnostic and Interventional Radiology (T.G.R., K.E., T.J.V.), University Hospital Frankfurt, Theodor-Stern-Kai 7, 60590 Frankfurt am Main, Germany; and Department of Biomedical Sciences and Morphological and Functional Imaging, University of Messina, Messina, Italy (T.D.). Received May 30, 2018; revision requested July 30; revision received August 27; accepted October 8. **Address correspondence to** J.L.W. (e-mail: *docwichmann@gmail.com*).

Conflicts of interest are listed at the end of this article.

Radiology 2018; 00:1–11 • https://doi.org/10.1148/radiol.2018181286 • Content codes: CT MK

Purpose: To assess the diagnostic performance of dual-energy CT with reconstruction of virtual noncalcium (VNCa) images for the detection of lumbar disk herniation compared with standard CT image reconstruction.

Materials and Methods: For this retrospective study, 41 patients (243 intervertebral disks; overall mean age, 68 years; 24 women [mean age, 68 years] and 17 men [mean age, 68 years]) underwent clinically indicated third-generation, dual-source, dual-energy CT and 3.0-T MRI within 2 weeks between March 2017 and January 2018. Six radiologists, blinded to clinical and MRI information, independently evaluated conventional grayscale dual-energy CT series for the presence and degree of lumbar disk herniation and spinal nerve root impingement. After 8 weeks, readers reevaluated examinations by using color-coded VNCa reconstructions. MRI evaluated by two separate experienced readers, blinded to clinical and dual-energy CT information, served as the standard of reference. Sensitivity and specificity were the primary metrics of diagnostic performance.

Results: A total of 112 herniated lumbar disks were depicted at MRI. VNCa showed higher overall sensitivity (612 of 672 [91%] vs 534 of 672 [80%]) and specificity (723 of 786 [92%] vs 665 of 786 [85%]) for detecting lumbar disk herniation compared with standard CT (all comparisons, $P < .001$). Interreader agreement was excellent for VNCa and substantial for standard CT ($\kappa = 0.82$ vs 0.67; $P < .001$). VNCa achieved superior diagnostic confidence, image quality, and noise scores compared with standard CT (all comparisons, $P < .001$).

Conclusion: Color-coded dual-energy CT virtual noncalcium reconstructions show substantially higher diagnostic performance and confidence for depicting lumbar disk herniation compared with standard CT.

Lumbar disk herniation is a frequent degenerative disorder, commonly causing lower back pain and entailing substantial social and economic burden (1–3). Complications such as compressions of the spinal cord or spinal nerve root can result in irreversible morbidity (4–6). Therefore, fast and accurate diagnosis is necessary for rapid initiation of optimal therapy and to avoid poor outcome (3).

MRI is the preferred diagnostic imaging modality due to its ability to provide excellent demarcation between intervertebral disk and cerebrospinal fluid (4). However, there are several potential limitations in clinical routine. The availability of MRI is usually limited outside of regular working hours. There are certain absolute and relative contraindications, including cochlear implants, pacemakers, claustrophobia, or the inability to lie still. Furthermore, MRI is relatively time-consuming and expensive (7). Thus, patients with severe back pain often initially undergo CT instead of MRI (8).

A large meta-analysis from 2012 (8) showed moderate sensitivity and specificity of standard CT for the detection of lumbar disk herniation. More recently, Notohamiprodjo et al (9) demonstrated improved results evaluating the diagnostic accuracy of single-energy CT compared with MRI with application of iterative reconstruction algorithms, although the detection of lumbar disk herniation remained challenging because of low contrast between intervertebral disk and cerebrospinal fluid.

Dual-energy CT has opened perspectives in imaging due to its ability for material characterization (10–14). In musculoskeletal dual-energy CT, virtual noncalcium (VNCa) images have been shown to allow for visualization of bone marrow edema (15–18). Such color-coded VNCa reconstructions have also been applied to dual-energy CT arthrography (13,19) and improved detection of bone marrow infiltration in patients with multiple myeloma (20). With the advent of third-generation, dual-source, dual-energy CT, VNCa reconstruction algorithms have been integrated in the postprocessing software. Thereby, a novel VNCa postprocessing algorithm optimized for colored imaging of lumbar disks by using two different color lookup tables has been established.

We hypothesized that color-coded VNCa images reconstructed from third-generation, dual-source, dual-energy

Abbreviations

NPV = negative predictive value, PPV = positive predictive value, VNCa = virtual noncalcium

Summary

Color-coded virtual noncalcium images optimized for the analysis of intervertebral disks show substantially higher diagnostic accuracy for the detection of lumbar disk herniation and spinal nerve root impingement in comparison to standard CT.

Implications for Patient Care

- Reconstruction of color-coded virtual noncalcium (VNCa) images from dual-energy CT took 4 minutes on average, showing potential applicability for routine clinical practice.
- Color-coded dual-energy VNCa CT images improve diagnostic accuracy for the detection of lumbar disk herniation and spinal nerve root impingement compared with standard CT.
- Dual-energy VNCa CT may serve as an alternative imaging approach for patients with contraindications to MRI or when MRI is unavailable.

CT may substantially improve diagnostic accuracy and confidence for the detection of lumbar disk herniation at noncontrast dual-energy CT in comparison to standard grayscale CT series, also due to the improved spectral separation with this scanner (21). Thus, the purpose of our study was to assess the diagnostic accuracy of a color-coded dual-energy CT VNCa reconstruction algorithm for the detection of lumbar disk herniation compared with standard CT by using MRI as the reference standard.

Materials and Methods

This retrospective study was approved by the institutional review board. The requirement to obtain written informed consent was waived. The institutional review board approved the chart review. Authors without conflicts of interest had full control of inclusion of any data and information submitted for publication.

Patient Selection and Study Design

Eighty-seven consecutive patients with acute lower back pain who had undergone clinically indicated and routinely performed noncontrast dual-energy CT and MRI of the lumbar spine between March 2017 and January 2018 were considered for inclusion. To limit possible distortion of the statistical correlation, we only included patients with an examination interval of up to 2 weeks (n = 64). We excluded patients with known malignancy of the spine (n = 9), with spondylodiskitis (n = 4), with dorsal instrumentation (n = 5), or with lumbar interbody spacers (n = 5). Two lumbar disks were excluded because of disk collapse due to lumbar block vertebra. One lumbar disk was excluded due to nucleotomy. Thus, 243 lumbar disks (Th12–S1) of 41 patients were ultimately evaluated (Fig 1).

Dual-Energy CT Protocol

Noncontrast CT examinations were performed by using a third-generation, dual-source, dual-energy CT system (Somatom Force; Siemens Healthineers, Forchheim, Germany). The two x-ray tubes were operated at different kilovoltage settings (tube A, 90 kVp and 220 mAs; tube B, Sn150 kVp [0.64-mm tin filter] and 138 mAs). CT was performed in craniocaudal direction with a dual-energy protocol (rotation time, 500 msec; pitch, 0.6; collimation, 128 × 0.6 mm). Automatic attenuation-based tube current modulation (CARE Dose 4D; Siemens Healthineers) was applied. Mean volume CT dose index ± standard deviation was 9.4 mGy ± 3.6 (range, 3.0–13.3 mGy) and mean dose-length product was 321.4 mGy · cm ± 64.5 (range, 86.6–789.1 mGy · cm).

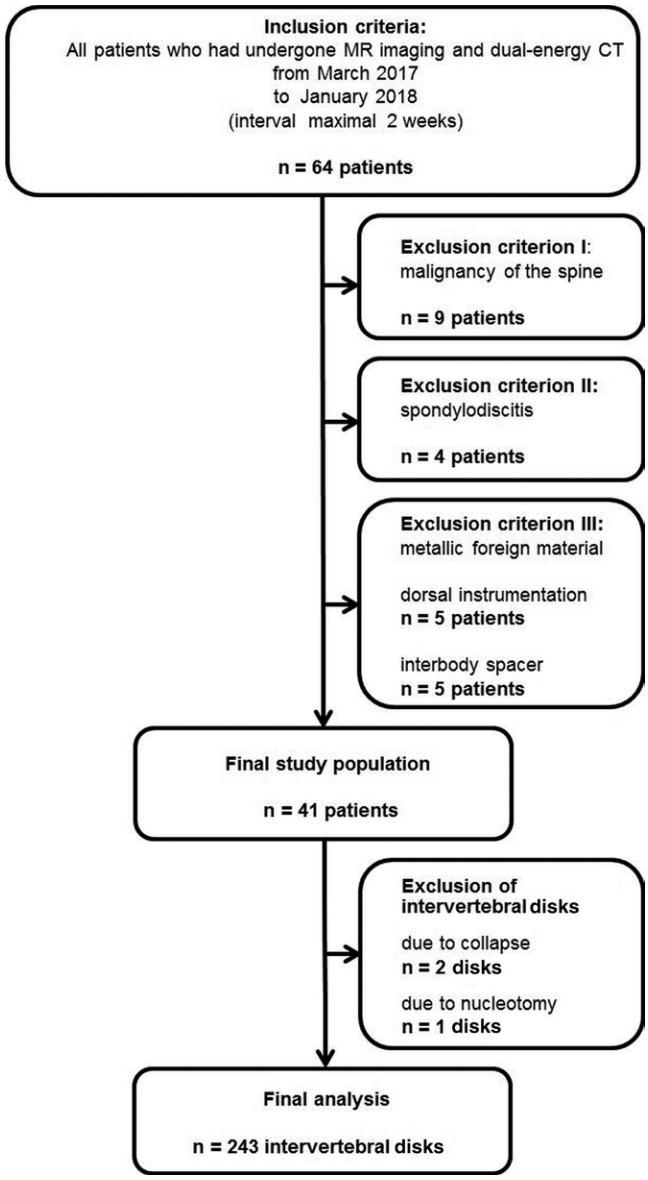

Figure 1: Flowchart shows selection of study population.

CT Image Reconstruction and Postprocessing

Three different image sets were acquired in each dual-energy CT scan: 90 kVp, Sn150 kVp, and weighted average (ratio, 0.5:0.5) to resemble the contrast properties of a single-energy 120-kVp image (22). Reconstructions (axial, section thickness of 2 mm and increment of 1 mm; sagittal, section thickness and increment of 2 mm) were created with a dedicated dual-energy medium-soft convolution kernel (Qr40, advanced model-based iterative reconstruction [ADMIRE] level of 3) for the high- and low-kilovolt

series. Postprocessing was performed with a commercially available three-dimensional workstation (syngo.via, version VB10B; Siemens Healthineers) with a three-material decomposition algorithm differentiating bone mineral, yellow marrow, and red marrow (23,24). A VNCa reconstruction algorithm optimized for analysis of intervertebral disks was applied by using dedicated software settings (color lookup tables low-energy value, spectrum; color lookup tables high-energy value, grayscale; CT preset 1, liver; CT preset 2, bone). For image analysis, the axial and sagittal VNCa reconstructions and standard CT series were sent to the picture archiving and communication system.

MRI Protocol

All patients underwent noncontrast MRI with a 3.0-T system (Magnetom PrismaFit; Siemens Healthineers) with a dedicated spine surface coil. Standard T1-weighted spin-echo (repetition time msec/echo time msec, 650/10; matrix size, 288 × 384; section thickness, 4 mm), T2-weighted fast spin-echo (4000/89; matrix size, 358 × 448; section thickness, 4 mm), and turbo inversion-recovery magnitude (3500/39; matrix size, 388 × 384; section thickness, 4 mm) sequences were performed in sagittal orientation. The T2-weighted sequence was also performed in axial plane.

Image Evaluation

Image evaluation was performed with a conventional picture archiving and communication system workstation (Centricity, version 4.2; GE Healthcare, Solingen, Germany). First, to set the standard of reference, two radiologists (K.E. and T.J.V., board-certified radiologists [managing consultant and head of department] with 20 years and 32 years of experience in musculoskeletal imaging, respectively), blinded to any clinical or dual-energy CT information, analyzed MRI series in consensus for the presence and degree of disk herniation according to the lumbar disk pathologic classification of the North American Spine Society (version 2.0) (25) and for the presence (grade 1 vs grade 2–4) of spinal nerve root impingement due to lumbar disks according to the Pfirrmann nerve root compression grading system (26). Each lumbar disk herniation, defined as a focal displacement of disk material (<25% of the disk circumference) beyond the limits of the intervertebral disk space, was classified as protrusion (distance between the edges of the disk herniation is less than the distance between the edges of the base), extrusion (distance between the edges of the herniated disk material is greater than the distance at the base in at least one plane), or sequestration (displaced disk material has lost continuity with the parent disk) by each reader. Bulging lumbar disks (disk tissue extending beyond the edges of the ring apophyses [>25% of the disk circumference]) were considered as nonherniated disks according to the nomenclature of the lumbar disk pathologic classification of the North American Spine Society (25). Regarding the detection of spinal nerve root impingement due to lumbar disks, each reader was asked to note every spinal nerve root impingement due to lumbar disks, whether due to bulging or herniated disks. Each reader was free to adjust window settings and to scroll through the whole stack of MRI series. Image quality, image noise, and diagnostic confidence were evaluated individually by using five-point Likert scales (1, unacceptable; 5, excellent) (9).

After definition of the reference standard, six radiologists with experience in musculoskeletal imaging (T.G.R., board-certified radiologist [consultant with special focus on musculoskeletal imaging] with 9 years of experience; J.L.W., board-certified radiologist with 6 years of experience; S.S.M., radiology resident with 5 years of experience; C.B., radiology resident with 3 years of experience; I.Y., radiology resident with 3 years of experience; J.N., senior-year medical student with 1 year of experience) who were blinded to the MRI results, indications, and clinical history independently reviewed axial and sagittal dual-energy CT series. First, conventional grayscale CT series were presented in random order. Readers were asked to report the presence and degree of all lumbar disk herniation and spinal nerve root impingement on a per-disk basis and on a per-patient basis. After an 8-week interval to avoid potential recall bias, readers evaluated color-coded VNCa reconstructions in random order without any access to grayscale CT data. Each reader was free to adjust window settings and to scroll through the whole stack of CT series. Image quality, image noise, and diagnostic confidence were evaluated in all CT series by using the aforementioned five-point Likert scales (9).

Statistical Analysis

Statistical analyses were conducted by using dedicated software (SPSS Statistics for Windows, version 23.0; IBM, Armonk, NY and MedCalc for Windows, version 13; MedCalc, Mariakerke, Belgium). Evaluation of normality of the data was performed by using the Kolmogorov-Smirnov test. Variables were expressed as means ± standard deviations and analyzed with the Wilcoxon matched-pairs test. A P value less than .05 was considered to indicate a statistically significant difference.

Sensitivity, specificity, positive predictive values (PPVs), negative predictive value (NPVs), and accuracy values were calculated on a per-patient basis, as well as on a per-disk basis. Clustering of intervertebral disks per patient following the method described by Genders et al (27) for each reader and for consensus reading on the basis of a contingency table was taken into account. Logistic regression analysis with a robust variance estimator was used. Sensitivity, specificity, PPV, and NPV between both CT algorithms were compared by using generalized estimating equations with an independent correlation working matrix and robust variance estimator to account for clustering of intervertebral disks per patient. Interreader agreement was evaluated by computing weighted Fleiss κ. All values of overall sensitivity, specificity, PPV, NPV, and accuracy are expressed as means. Mean ages are expressed as patient-level means.

Results

A total of 243 lumbar intervertebral disks (median per patient, six; range, five to six) in 41 patients (mean age, 68 years ± 14; range, 35–92 years; mean body mass index, 25 kg/m^2 ± 3; range, 17–34 kg/m^2) were finally included, consisting of 17 men (41%; mean age, 68 years ± 12; range, 50–92 years; mean body mass index, 25 kg/m^2 ± 3; range, 19–30 kg/m^2) and 24 women (59%; mean age, 68 years ± 16; range, 35–91 years; mean body mass index, 27 kg/m^2 ± 5; range, 17–34 kg/m^2) (Table 1). Six patients (15%) had known lumbar disk herniation, eight patients (20%) had known osteoporosis, and five patients (12%)

had scoliosis of the lumbar spine. MRI revealed 112 lumbar herniated disks (46% of all intervertebral disks; median per patient, three; range, zero to six) and 29 instances of spinal nerve root impingement. According to the classification of the North American Spine Society, lumbar disk herniations were classified as 58 protrusions (24%), 51 extrusions (21%), and three sequestrations (1%) (25). Mean examination interval between dual-energy CT and MRI was 4 days (range, 0–13 days).

Diagnostic Accuracy per Patient

The analysis per patient showed higher overall sensitivity (169 of 174 [97%] vs 146 of 174 [84%]), specificity (53 of 72 [74%] vs 25 of 72 [35%]), PPV (169 of 188 [90%] vs 146 of 193 [76%]), NPV (53 of 58 [91%] vs 25 of 53 [47%]), and accuracy (222 of 246 [90%] vs 171 of 246 [70%]) of color-coded VNCa reconstructions for the detection of lumbar disk protrusion according to the classification of the North American Spine Society compared with standard CT images (all comparisons, $P < .001$) (25). An example case demonstrating improvement in detecting lumbar disk protrusion by using VNCa reconstructions is illustrated in Figure 2.

For the detection of spinal nerve root impingement, VNCa images yielded higher overall sensitivity (92 of 96 [96%] vs 82 of 96 [85%]), specificity (143 of 150 [95%] vs 130 of 150 [87%]), PPV (92 of 99 [93%] vs 82 of 102 [80%]), NPV (143 of 147 [97%] vs 130 of 143 [90%]), and accuracy (235 of 246 [96%] vs 212 of 246 [86%]) compared with standard CT (all comparisons, $P < .001$) (Table 2). Interreader agreement was good for VNCa reconstructions and moderate for standard CT images regarding the detection of lumbar disk protrusion ($\kappa = 0.75$ vs 0.46), good and moderate for detecting lumbar disk extrusion ($\kappa = 0.69$ vs 0.41), excellent and moderate for detecting lumbar disk sequestration ($\kappa = 0.94$ vs 0.41), and excellent and only moderate for detecting spinal nerve root impingement ($\kappa = 0.87$ vs 0.56) (all comparisons, $P < .001$).

Diagnostic Accuracy per Intervertebral Disk

Color-coded VNCa reconstructions showed higher overall sensitivity (612 of 672 [91%] vs 534 of 672 [80%]), specificity (723 of 786 [92%] vs 665 of 786 [85%]), PPV (612 of 675 [91%] vs 534 of 655 [82%]), NPV (655 of 803 [83%] vs 665 of 803 [83%]), and accuracy (1335 of 1458 [92%] vs 1199 of 1458 [82%]) for the detection of lumbar disk herniation compared with standard CT images taking clustering into account (all comparisons, $P < .001$). Interreader agreement was excellent for VNCa images ($\kappa = 0.82$) and substantial for standard CT ($\kappa = 0.67$) ($P < .001$).

Regarding the classification of the North American Spine Society (25), the statistical analysis revealed higher overall sensitivity (288 of 348 [83%] vs 247 of 348 [71%]), specificity (986 of 1110 [89%] vs 845 of 1110 [76%]), PPV (288 of 412 [70%] vs 247 of 512 [48%]), NPV (986 of 1046 [94%] vs 845 of 946 [89%]), and accuracy (1274 of 1458 [87%] vs 1092 of 1458 [75%]) for the detection of lumbar disk protrusion by using VNCa reconstructions compared with standard CT taking clustering into account (all comparisons, $P < .001$) (Table 3). Interreader agreement was excellent for VNCa images ($\kappa = 0.81$) but only moderate for standard CT ($\kappa = 0.48$) ($P < .001$).

Table 1: Characterization of the Patient Population ($n = 41$)

Characteristic	Value
Overall age (y)	68 ± 14 (35–92)
Overall BMI (kg/m^2)	25 ± 3 (17–34)
Women	24/41 (59)*
Age (y)	68 ± 16 (35–91)
BMI (kg/m^2)	27 ± 5 (17–34)
Men	17/41 (41)*
Age (y)	68 ± 12, 50–92
BMI (kg/m^2)	23 ± 3, 19–30
No. of patients with known lumbar disk herniation*	6/41 (15)
No. of patients with known osteoporosis*	8/41 (20)
No. of patients with known scoliosis*	5/41 (12)

Note.—Unless otherwise specified, data are means ± standard deviation, with ranges in parentheses. BMI = body mass index.

* Data are numerators and denominators, with percentages in parentheses.

For the detection of spinal nerve root impingement VNCa reconstructions yielded higher overall sensitivity (160 of 174 [92%] vs 119 of 174 [68%]), specificity (1261 of 1284 [98%] vs 1233 of 1284 [96%]), PPV (160 of 183 [87%] vs 119 of 179 [70%]), NPV (1261 of 1275 [99%] vs 1233 of 1288 [96%]), and accuracy (1421 of 1458 [97%] vs 1352 of 1458 [93%]) compared with standard CT taking clustering into account (all comparisons, $P < .001$). Interreader agreement was good for VNCa images ($\kappa = 0.79$) and moderate for standard CT ($\kappa = 0.46$). An example case showing facilitated assessment of spinal nerve root impingement by using VNCa reconstructions compared with standard CT is shown in Figure 3.

Comparing all CT readers (T.G.R., J.L.W., S.S.M., C.B., I.Y., J.N.), the least experienced reader (J.N.) showed the most distinct improvement regarding diagnostic accuracy by using VNCa reconstructions with higher overall sensitivity (101 of 112 [90%] vs 70 of 112 [63%]), specificity (118 of 131 [90%] vs 98 of 131 [75%]), PPV (101 of 114 [89%] vs 70 of 103 [68%]), NPV (118 of 129 [92%] vs 98 of 140 [70%]), and accuracy (219 of 243 [90%] vs 168 of 243 [69%]) for the detection of lumbar disk herniation (all comparisons, $P < .001$), as well as higher overall sensitivity (28 of 29 [97%] vs 19 of 29 [66%]), specificity (208 of 214 [97%] vs 199 of 214 [93%]), PPV (28 of 34 [82%] vs 19 of 34 [56%]), NPV (210 of 213 [99%] vs 199 of 209 [95%]), and accuracy (236 of 243 [97%] vs 218 of 243 [90%]) for detecting spinal nerve root impingement (all comparisons, $P < .001$). The most experienced reader (T.G.R.) was able to achieve similar diagnostic performance in the detection of lumbar disk herniation as with MRI with an overall sensitivity of 96% (107 of 112), specificity of 95% (124 of 131), PPV of 94% (107 of 114), NPV of 96% (124 of 129), and accuracy of 95% (231 of 243). All other CT readers achieved higher sensitivity, specificity, PPV, NPV, and accuracy (all comparisons, $P < .001$) for the detection of lumbar disk herniation and spinal nerve root impingement by using VNCa reconstructions compared with standard CT (Tables 4, 5).

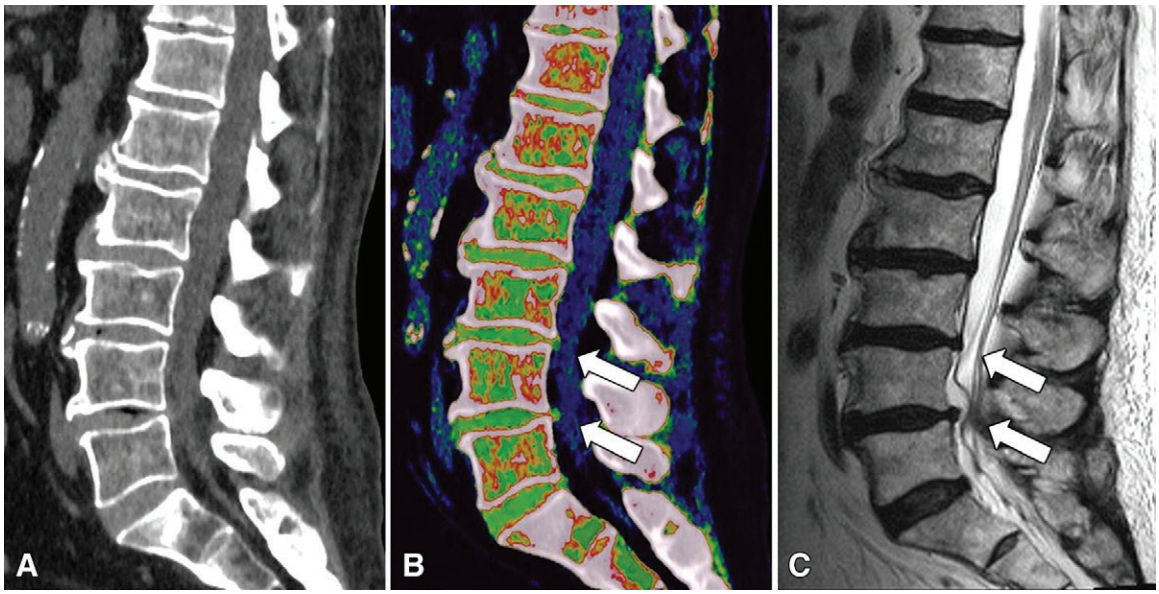

Figure 2: Images in a 65-year-old man who presented with acute severe lower back pain after lifting heavy bags. *A,* At standard noncontrast CT, lumbar disk protrusions L3/L4 and L4/L5 were initially not clearly depicted on sagittal grayscale reconstructions. *B,* Both lumbar disk protrusions (arrows) were detected by all readers after reconstruction of sagittal virtual noncalcium images optimized for analysis of intervertebral disks. *C,* Additional noncontrast MRI confirmed diagnosis at sagittal T2-weighted series.

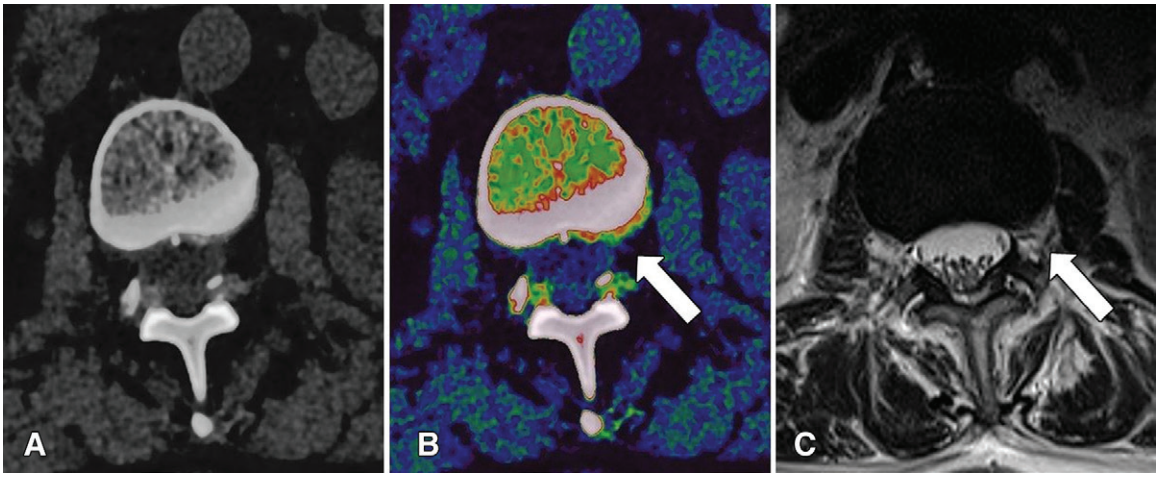

Figure 3: Images in a 62-year-old woman with known osteoporosis who presented with lower back pain, paresthesia in left lower leg, and paralysis of left extensor hallucis longus muscle. *A,* Nerve root impingement of bulging intervertebral disk L4/L5 on left side was underestimated at standard noncontrast axial CT series by four of six readers. *B,* Diagnosis of left grade 2 spinal nerve root impingement (arrow) according to Pfirrmann nerve root compression grading system was made by all readers after reconstruction of axial color-coded virtual noncalcium images. *C,* Extent of spinal nerve root impingement was confirmed by additionally obtained MRI at axial T2-weighted series (arrow).

Diagnostic Confidence

Regarding the diagnosis of lumbar disk herniation, readers showed very high confidence for all MRI series (mean score, 4.85), whereas the diagnostic confidence for VNCa reconstructions was similarly high (mean score, 4.80) (P = .22) (Fig 4). In contrast, readers' scores indicated lower confidence when analyzing standard CT images compared with VNCa reconstructions (mean score, 2.87) ($P < .001$). Interreader agreement was good for VNCa images (κ = 0.71), as well as for standard CT (κ = 0.61).

The image noise in MRI series was rated with a mean score of 4.37 and in VNCa reconstructions with a mean score of 4.31, implicating similarly low noise levels in these examinations (P = .26). In comparison to standard CT images (mean score, 3.06), the readers perceived less noise on VNCa reconstructions ($P < .001$). Interreader agreement was excellent for VNCa images (κ = 0.82) and good for standard CT (κ = 0.74).

The image quality was rated with a mean score of 4.51 for MRI and a mean score of 4.48 for VNCa reconstructions, yielding no difference between both techniques (P = .40). In contrast, readers rated the image quality in standard CT images lower in comparison to VNCa reconstructions with a mean score of 3.10 ($P < .001$). Interreader agreement was excellent

Table 2: Diagnostic Accuracy of Standard CT and Color-coded VNCa Reconstructions per Patient

Parameter	Sensitivity (%)	Specificity (%)	PPV (%)	NPV (%)	Accuracy (%)
Lumbar disk protrusion					
Standard CT	146/174 (84) [80, 88]	25/72 (35) [24, 47]	146/193 (76) [74, 81]	25/53 (47) [27, 63]	171/246 (70) [59, 82]
VNCa	169/174 (97) [93, 99]	53/72 (74) [62, 83]	169/188 (90) [86, 93]	53/58 (91) [82, 96]	222/246 (90) [84, 96]
Lumbar disk extrusion					
Standard CT	68/156 (44) [36, 52]	77/90 (86) [78, 91]	68/81 (84) [75, 90]	77/165 (47) [43, 51]	145/246 (59) [42, 75]
VNCa	135/156 (87) [77, 92]	79/90 (88) [79, 94]	135/146 (93) [87, 97]	79/100 (79) [70, 86]	214/246 (87) [80, 92]
Lumbar disk sequestration					
Standard CT	4/18 (22) [6, 48]	217/218 (95) [92, 98]	4/15 (27) [11, 51]	217/231 (94) [92, 95]	221/246 (90) [85, 95]
VNCa	18/18 (100)	227/228 (100) [96, 100]	18/19 (95) [93, 98]	227/227 (100)	245/246 (100) [99, 100]
Spinal nerve root impingement					
Standard CT	82/96 (85) [77, 92]	130/150 (87) [80, 92]	82/102 (80) [73, 87]	130/143 (90) [85, 94]	212/246 (86) [81, 90]
VNCa	92/96 (96) [90, 99]	143/150 (95) [91, 98]	92/99 (93) [86, 96]	143/147 (97) [93, 99]	235/246 (96) [90, 99]

Note.—MRI served as the standard of reference. Denominators represent the total number with respect to the respective statistical measure. Data in brackets are 95% confidence intervals. NPV = negative predictive value, PPV = positive predictive value, VNCa = virtual noncalcium.

Table 3: Diagnostic Accuracy of Standard CT and Color-coded VNCa Reconstructions for the Classification of Lumbar Disk Herniation per Intervertebral Disk

Parameter	Sensitivity (%)	Specificity (%)	PPV (%)	NPV (%)	Accuracy (%)
Lumbar disk protrusion					
Standard CT	247/348 (71) [64, 81]	845/1110 (76) [70, 83]	247/512 (48) [38, 57]	845/946 (89) [83, 94]	1092/1458 (75) [66, 85]
VNCa	288/348 (83) [74, 94]	986/1110 (89) [82, 96]	288/412 (70) [60, 79]	986/1046 (94) [89, 97]	1274/1458 (87) [79, 95]
Lumbar disk extrusion					
Standard CT	95/306 (31) [22, 43]	1120/1252 (97) [94, 99]	95/127 (75) [66, 86]	1120/1331 (84) [75, 94]	1215/1458 (83) [74, 92]
VNCa	255/306 (83) [78, 89]	1126/1152 (98) [96, 100]	255/281 (91) [82, 97]	1126/1177 (96) [90, 100]	1387/1458 (95) [90, 99]
Lumbar disk sequestration					
Standard CT	4/18 (22) [11, 34]	1371/1440 (95) [90, 99]	4/73 (6) [2, 11]	1371/1385 (99) [97, 100]	1375/1458 (94) [88, 98]
VNCa	18/18 (100)	1438/1440 (100) [98, 100]	18/20 (90) [80, 97]	1438/1438 (100)	1448/1458 (99) [97, 100]

Note.—Classification of lumbar disk protrusion, extrusion, and sequestration per intervertebral disk is according to the lumbar disk pathologic classification of the North American Spine Society, with MRI as the standard of reference taking into account clustering. Source.—Reference 25. Statistical analysis revealed improved diagnostic accuracy of virtual noncalcium (VNCa) reconstructions compared with standard CT images for correct classification of lumbar disk herniation. Denominators represent the total number with respect to the respective statistical measure. Data in brackets are 95% confidence intervals. NPV = negative predictive value, PPV = positive predictive value.

for VNCa ($\kappa = 0.81$) and good for standard CT ($\kappa = 0.73$) ($P < .001$).

Discussion

Our study results showed color-coded VNCa reconstructions had substantially higher diagnostic accuracy compared with standard CT for depiction of lumbar disk herniation and spinal nerve root impingement. Color-coded VNCa reconstructions yielded high overall sensitivity, specificity, PPV, and NPV (all >90%) for detecting lumbar disk herniation. Notably, the most inexperienced reader (J.N.) showed the most distinct improvement by using VNCa reconstructions, as particularly

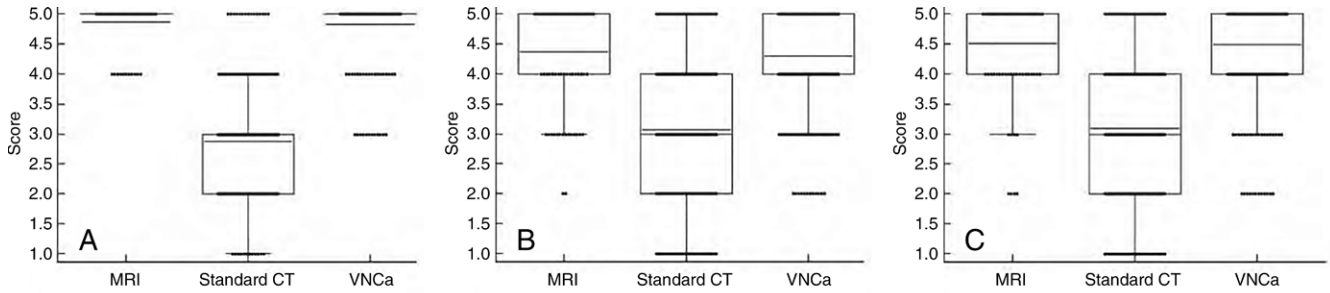

Figure 4: Box and dot plots demonstrate qualitative assessment of, *A,* diagnostic confidence, *B,* amount of noise and, *C,* image quality of MRI, standard CT, and color-coded virtual noncalcium (VNCa) reconstructions in the study. Mean scores are shown as horizontal black lines and dots show distribution of scores. Color-coded VNCa reconstructions achieved significantly higher mean scores than did standard CT images for all categories (all $P < .001$). Regarding comparison of optimized VNCa reconstructions and MRI series, no significant difference was found in diagnostic confidence ($P = .22$), amount of noise ($P = .26$), and image quality ($P = .40$) between both approaches.

sensitivity (101 of 112 [90%] vs 70 of 112 [63%]) and PPV (101 of 114 [89%] vs 98 of 131 [75%]) could be substantially improved. For the most experienced reader (T.G.R.), the color-coded VNCa reconstructions enabled similar diagnostic accuracy as with MRI. In addition, VNCa images achieved similar ratings for diagnostic confidence, image quality, and noise without significant differences compared with MRI. Importantly, our data demonstrated superior ratings for VNCa regarding all categories in comparison to standard CT. Furthermore, significantly higher interreader agreement in detecting lumbar disk herniation and spinal nerve root impingement compared with standard CT indicates the greater reliability of VNCa reconstructions.

Previous studies (8,9) showed moderate diagnostic accuracy of conventional grayscale CT for the detection of lumbar disk herniation. Dual-energy CT allows for three-material decomposition and calculation of color-coded VNCa images by using energy dependence of the photoelectric effect at different x-ray spectra, resulting in improved tissue quantification and differentiation by its atomic number (28). Thereby, the relatively high density and material composition of intervertebral disks compared with other soft-tissue structures permits visualization by using optimized VNCa reconstructions. However, to our knowledge, no studies have reported on the usage of color-coded VNCa reconstructions to improve the contrast between intervertebral disks and cerebrospinal fluid and therefore to visualize lumbar intervertebral disks to date.

The observed high diagnostic accuracy of VNCa reconstructions for the detection of lumbar disk herniation in our study emphasizes the potential role of dual-energy CT as an appropriate alternative imaging approach for patients with contraindications to MRI or in circumstances where MRI is not available. Our data also suggest that VNCa reconstructions may serve as an alternative imaging approach for depicting spinal nerve root impingement, because sensitivity and PPV could be distinctly higher compared with standard CT. Particularly inexperienced readers, such as radiologic residents in their first years, could substantially benefit from VNCa reconstructions, as the most inexperienced reader in this study showed the most benefit using VNCa reconstructions for the detection of lumbar disk herniation compared with standard CT (especially sensitivity showed the most distinct improvement). In addition, we observed that readers showed the most improvement by using VNCa reconstructions for the detection of lumbar disk herniation in general in cases of small protrusions due to color-coded visualization of lumbar disks and excellent demarcation between lumbar disks and cerebrospinal fluid compared with grayscale CT. Regarding the correct classification of lumbar disk herniations, readers showed the most benefit using VNCa reconstructions in cases of extrusions and sequestrations compared with standard CT. No difference was found in the ability to detect lumbar disk herniation based on the body mass index of the patients in this study. Several studies showed high diagnostic accuracy of VNCa reconstructions for the detection of bone marrow edema, so dual-energy CT may provide more detailed combined information of osseous and disk pathologies of the lumbar spine compared with standard CT (16–18). We noticed that color-coded VNCa reconstructions showed lower diagnostic accuracy in patients with degenerative lumbar spine in comparison to patients without degenerations due to overlap problems by degenerative osseous alterations adjacent to lumbar disks in this study; therefore, we conclude VNCa reconstructions provide the highest diagnostic accuracy in patients without degenerative osseous alterations of the lumbar spine like younger patients. This may be subject to future research, also to optimize the postprocessing algorithm for patients with degenerative spine alterations, which represent a large proportion of the patient population. Reconstruction of color-coded VNCa images from dual-energy CT took only 4 minutes on average, so we believe the reconstruction algorithm is applicable for routine clinical practice.

There were certain limitations to our study that warrant discussion. First, due to the retrospective single-center study design and an examination interval of up to 2 weeks between dual-energy CT and MRI, only 41 patients were ultimately included. A multicenter approach with a larger patient group is required to reassess the results of our study. Second, MRI was chosen as the standard of reference for the diagnosis of lumbar disk herniation. Some previous studies evaluating the diagnostic accuracy of standard CT for diagnosing lumbar spine pathologies used surgery as standard of reference (9), because MRI may also overestimate the degree of disk herniation and

Table 4: Comparison of Diagnostic Accuracy of All Readers for the Detection of Lumbar Disk Herniation per Intervertebral Disk

Parameter	Sensitivity (%)	Specificity (%)	PPV (%)	NPV (%)	Accuracy (%)
Average					
Standard CT	534/672 (80) [76, 83]	665/786 (85) [82, 87]	534/655 (82) [79, 84]	665/803 (83) [81, 85]	1199/1458 (82) [75, 86]
VNCa	612/672 (91) [89, 93]	723/786 (92) [90, 94]	612/675 (91) [89, 93]	723/783 (92) [90, 94]	1335/1458 (92) [88, 96]
Reader 1					
Standard CT	70/112 (63) [52, 71]	98/131 (75) [67, 90]	70/103 (68) [70, 85]	98/140 (70) [67, 77]	168/243 (69) [62, 76]
VNCa	101/112 (90) [85, 94]	118/131 (90) [87, 94]	101/114 (89) [86, 95]	118/129 (92) [88, 94]	219/243 (90) [84, 96]
Reader 2					
Standard CT	92/112 (82) [72, 84]	114/131 (87) [84, 91]	92/109 (84) [80, 88]	114/134 (85) [73, 90]	206/243 (85) [80, 90]
VNCa	99/112 (88) [83, 95]	119/131 (91) [87, 95]	99/111 (89) [82, 92]	119/132 (90) [84, 95]	218/243 (90) [86, 95]
Reader 3					
Standard CT	100/112 (89) [83, 91]	119/131 (91) [84, 94]	100/112 (89) [84, 92]	119/131 (91) [85, 94]	219/243 (90) [84, 94]
VNCa	104/112 (93) [87, 96]	125/131 (95) [90, 98]	104/110 (95) [89, 98]	125/133 (94) [90, 97]	229/243 (94) [90, 97]
Reader 4					
Standard CT	99/112 (88) [84, 91]	106/131 (81) [75, 86]	99/124 (80) [74, 85]	106/119 (89) [81, 93]	205/243 (84) [78, 88]
VNCa	101/112 (90) [87, 94]	115/131 (88) [84, 92]	101/117 (86) [80, 90]	115/126 (91) [86, 95]	216/243 (89) [85, 95]
Reader 5					
Standard CT	78/112 (70) [60, 78]	111/131 (85) [80, 90]	78/98 (80) [72, 87]	111/145 (77) [70, 83]	189/243 (78) [70, 85]
VNCa	100/112 (89) [83, 95]	122/131 (93) [88, 96]	100/109 (92) [86, 97]	122/134 (91) [87, 95]	222/243 (91) [86, 95]
Reader 6					
Standard CT	95/112 (85) [80, 90]	117/131 (89) [81, 95]	95/109 (87) [78, 93]	117/134 (87) [83, 91]	212/243 (87) [80, 90]
VNCa	107/112 (96) [92, 99]	124/131 (95) [91, 98]	107/114 (94) [90, 97]	124/129 (96) [91, 98]	213/243 (95) [91, 98]

Note.—Diagnostic accuracy of standard CT and color-coded virtual noncalcium (VNCa) reconstructions for the detection of lumbar disk herniation per intervertebral disk with MRI as standard of reference taking into account clustering. Notably, the most experienced reader (reader 6, a board-certified radiologist with special focus on musculoskeletal [MSK] imaging and 9 years of experience) was able to achieve similar diagnostic performance in the detection of lumbar disk herniation by using VNCa reconstructions as with MRI. Reader 1 had 1 year of experience in MSK imaging, reader 2 had 3 years, reader 3 had 3 years, reader 4 had 5 years, and reader 5 had 6 years. Denominators represent the total number with respect to the respective statistical measure. Data in brackets are 95% confidence intervals. NPV = negative predictive value, PPV = positive predictive value.

spinal nerve root impingement (29,30). Third, the results of our study are currently only applicable to the vendor-specific CT system and postprocessing software, although dual-energy CT is offered by all major vendors. Fourth, conventional gray-scale CT series were evaluated initially followed by image analysis of VNCa reconstructions after 8 weeks in all cases instead of randomizing this sequence, possibly leading to recall bias and statistical distortion.

In conclusion, our study showed that a color-coded dual-energy CT virtual noncalcium (VNCa) reconstruction algorithm yielded substantially improved diagnostic accuracy for the detection of lumbar disk herniation and spinal nerve root impingement compared with conventional CT by using MRI as the reference standard. Inexperienced readers showed the most benefit using this algorithm, whereas the most experienced reader was able to achieve diagnostic performance similar to that of MRI. Furthermore, diagnostic confidence, image quality, and noise scores were equivalent for VNCa and MR images. Therefore, we believe this algorithm can potentially become a viable alternative when MRI is unavailable but dual-energy CT can be performed.

Acknowledgment: The authors thank Dimitra Bon, PhD, for statistical consultation and assistance.

Table 5: Comparison of Diagnostic Accuracy of All Readers for the Detection of Spinal Nerve Root Impingement per Intervertebral Disk

Parameter	Sensitivity (%)	Specificity (%)	PPV (%)	NPV (%)	Accuracy (%)
Average					
Standard CT	119/174 (68) [62, 76]	1233/1284 (96) [94, 97]	119/170 (70) [64, 76]	1233/1288 (96) [92, 98]	1352/1458 (93) [88, 95]
VNCa	160/174 (92) [87, 96]	1261/1284 (98) [97, 99]	160/183 (87) [82, 91]	1261/1275 (99) [98, 99]	1421/1458 (97) [96, 99]
Reader 1					
Standard CT	19/29 (66) [53, 78]	199/214 (93) [91, 96]	19/34 (56) [44, 69]	199/209 (95) [93, 98]	218/243 (90) [84, 94]
VNCa	28/29 (97) [87, 99]	208/224 (97) [94, 99]	28/34 (82) [68, 99]	208/209 (100) [97, 100]	236/243 (97) [95, 99]
Reader 2					
Standard CT	23/29 (79) [70, 87]	208/214 (97) [94, 99]	23/29 (79) [71, 86]	208/214 (97) [93, 98]	231/243 (95) [90, 97]
VNCa	26/29 (90) [82, 99]	210/214 (98) [95, 99]	26/30 (87) [77, 91]	210/213 (99) [96, 100]	236/243 (97) [92, 100]
Reader 3					
Standard CT	14/29 (48) [35, 62]	209/214 (98) [93, 99]	14/19 (74) [64, 79]	209/224 (93) [89, 96]	223/243 (92) [88, 95]
VNCa	26/29 (90) [84, 97]	212/214 (99) [95, 100]	26/28 (90) [82, 96]	212/215 (99) [97, 100]	238/243 (98) [95, 100]
Reader 4					
Standard CT	21/29 (72) [59, 78]	205/214 (96) [92, 98]	21/30 (70) [62, 81]	205/213 (96) [93, 98]	226/243 (93) [88, 96]
VNCa	26/30 (90) [85, 96]	210/214 (98) [96, 100]	26/30 (87) [82, 93]	210/213 (99) [97, 100]	236/243 (97) [95, 100]
Reader 5					
Standard CT	23/29 (79) [70, 84]	207/214 (97) [96, 99]	23/30 (77) [60, 84]	207/213 (97) [93, 99]	230/243 (95) [88, 98]
VNCa	27/29 (93) [82, 99]	211/214 (99) [98, 100]	27/30 (90) [86, 95]	211/213 (99) [98, 100]	238/243 (98) [95, 100]
Reader 6					
Standard CT	24/29 (83) [64, 94]	205/214 (96) [92, 98]	24/33 (73) [60, 84]	205/210 (98) [95, 99]	229/243 (94) [90, 97]
VNCa	27/29 (93) [80, 99]	210/214 (98) [95, 100]	27/31 (87) [72, 95]	210/212 (99) [97, 100]	237/243 (98) [97, 100]

Note.—Diagnostic accuracy of standard CT and color-coded virtual noncalcium (VNCa) reconstructions for the detection of spinal nerve root impingement per intervertebral disk is according to the Pfirrmann nerve root compression grading system, with MRI as standard of reference taking into account clustering. Source.—Reference 26. The least experienced reader (reader 1, with 1 year of experience in musculoskeletal [MSK] imaging) showed the most distinct improvement regarding diagnostic accuracy by using VNCa reconstructions. Reader 2 had 3 years of experience in MSK imaging, reader 3 had 3 years, reader 4 had 5 years, reader 5 had 6 years, and reader 6 had 9 years. Denominators represent the total number with respect to the respective statistical measure. Data in brackets are 95% confidence intervals. NPV = negative predictive value, PPV = positive predictive value.

Author contributions: Guarantors of integrity of entire study, C.B., M.H.A., J.L.W.; study concepts/study design or data acquisition or data analysis/interpretation, all authors; manuscript drafting or manuscript revision for important intellectual content, all authors; approval of final version of submitted manuscript, all authors; agrees to ensure any questions related to the work are appropriately resolved, all authors; literature research, C.B., S.S.M., M.H.A., I.Y., L.L., T.D., J.L.W.; clinical studies, C.B., J.N., M.H.A., I.Y., T.G.R., K.E., T.D., T.J.V., J.L.W.; statistical analysis, C.B., S.S.M., M.H.A., I.Y.; and manuscript editing, C.B., S.S.M., M.H.A., I.Y., T.J.V., J.L.W.

Disclosures of Conflicts of Interest: **C.B.** disclosed no relevant relationships. **J.N.** disclosed no relevant relationships. **S.S.M.** disclosed no relevant relationships. **M.H.A.** Activities related to the present article: disclosed no relevant relationships. Activities not related to the present article: received speaker fees from Siemens. Other relationships: disclosed no relevant relationships. **I.Y.** disclosed no relevant relationships. **L.L.** disclosed no relevant relationships. **T.G.R.** disclosed no relevant relationships. **K.E.** disclosed no relevant relationships. **T.D.** disclosed no relevant relationships. **T.J.V.** disclosed no relevant relationships. **J.L.W.** Activities related to the present article: disclosed no relevant relationships. Activities not related to the present article: received payment for lectures including service on speakers bureaus from GE Healthcare and Siemens Healthineers. Other relationships: disclosed no relevant relationships.

References

1. Burton AK, Balagué F, Cardon G, et al. Chapter 2. European guidelines for prevention in low back pain: November 2004. Eur Spine J 2006;15(Suppl 2):S136–S168.
2. Saleem S, Aslam HM, Rehmani MAK, Raees A, Alvi AA, Ashraf J. Lumbar disc degenerative disease: disc degeneration symptoms and magnetic resonance image findings. Asian Spine J 2013;7(4):322–334.
3. Chou R, Qaseem A, Snow V, et al. Diagnosis and treatment of low back pain: a joint clinical practice guideline from the American College of Physicians and the American Pain Society. Ann Intern Med 2007;147(7):478–491.

4. Airaksinen O, Brox JI, Cedraschi C, et al. Chapter 4. European guidelines for the management of chronic nonspecific low back pain. Eur Spine J 2006;15(Suppl 2):S192–S300.
5. Bečulić H, Skomorac R, Jusić A, et al. Impact of timing on surgical outcome in patients with cauda equina syndrome caused by lumbar disc herniation. Med Glas (Zenica) 2016;13(2):136–141.
6. Small SA, Perron AD, Brady WJ. Orthopedic pitfalls: cauda equina syndrome. Am J Emerg Med 2005;23(2):159–163.
7. Morsbach F, Desbiolles L, Raupach R, Leschka S, Schmidt B, Alkadhi H. Noise texture deviation: a measure for quantifying artifacts in computed tomography images with iterative reconstructions. Invest Radiol 2017;52(2):87–94.
8. van Rijn RM, Wassenaar M, Verhagen AP, et al. Computed tomography for the diagnosis of lumbar spinal pathology in adult patients with low back pain or sciatica: a diagnostic systematic review. Eur Spine J 2012;21(2):228–239.
9. Notohamiprodjo S, Stahl R, Braunagel M, et al. Diagnostic accuracy of contemporary multidetector computed tomography (MDCT) for the detection of lumbar disc herniation. Eur Radiol 2017;27(8):3443–3451.
10. Nicolaou S, Liang T, Murphy DT, Korzan JR, Ouellette H, Munk P. Dual-energy CT: a promising new technique for assessment of the musculoskeletal system. AJR Am J Roentgenol 2012;199(5 Suppl):S78–S86.
11. Nicolaou S, Yong-Hing CJ, Galea-Soler S, Hou DJ, Louis L, Munk P. Dual-energy CT as a potential new diagnostic tool in the management of gout in the acute setting. AJR Am J Roentgenol 2010;194(4):1072–1078.
12. Wichmann JL, Booz C, Wesarg S, et al. Dual-energy CT-based phantomless in vivo three-dimensional bone mineral density assessment of the lumbar spine. Radiology 2014;271(3):778–784.
13. Mallinson PI, Coupal TM, McLaughlin PD, Nicolaou S, Munk PL, Ouellette HA. Dual-energy CT for the musculoskeletal system. Radiology 2016;281(3):690–707.
14. Gruber M, Bodner G, Rath E, Supp G, Weber M, Schueller-Weidekamm C. Dual-energy computed tomography compared with ultrasound in the diagnosis of gout. Rheumatology (Oxford) 2014;53(1):173–179.
15. Pache G, Krauss B, Strohm P, et al. Dual-energy CT virtual noncalcium technique: detecting posttraumatic bone marrow lesions—feasibility study. Radiology 2010;256(2):617–624.
16. Petritsch B, Kosmala A, Weng AM, et al. Vertebral compression fractures: third-generation dual-energy CT for detection of bone marrow edema at visual and quantitative analyses. Radiology 2017;284(1):161–168.
17. Kaup M, Wichmann JL, Scholtz JE, et al. Dual-energy CT–based display of bone marrow edema in osteoporotic vertebral compression fractures: impact on diagnostic accuracy of radiologists with varying levels of experience in correlation to MR imaging. Radiology 2016;280(2):510–519.
18. Wang CK, Tsai JM, Chuang MT, Wang MT, Huang KY, Lin RM. Bone marrow edema in vertebral compression fractures: detection with dual-energy CT. Radiology 2013;269(2):525–533.
19. Chai JW, Choi JA, Choi JY, Kim S, Hong SH, Kang HS. Visualization of joint and bone using dual-energy CT arthrography with contrast subtraction: in vitro feasibility study using porcine joints. Skeletal Radiol 2014;43(5):673–678.
20. Kosmala A, Weng AM, Heidemeier A, et al. Multiple myeloma and dual-energy CT: diagnostic accuracy of virtual noncalcium technique for detection of bone marrow infiltration of the spine and pelvis. Radiology 2018;286(1):205–213.
21. Krauss B, Grant KL, Schmidt BT, Flohr TG. The importance of spectral separation: an assessment of dual-energy spectral separation for quantitative ability and dose efficiency. Invest Radiol 2015;50(2):114–118.
22. Albrecht MH, Trommer J, Wichmann JL, et al. Comprehensive comparison of virtual monoenergetic and linearly blended reconstruction techniques in third-generation dual-source dual-energy computed tomography angiography of the thorax and abdomen. Invest Radiol 2016;51(9):582–590.
23. Nickoloff EL, Feldman F, Atherton JV. Bone mineral assessment: new dual-energy CT approach. Radiology 1988;168(1):223–228.
24. Liu X, Yu L, Primak AN, McCollough CH. Quantitative imaging of element composition and mass fraction using dual-energy CT: three-material decomposition. Med Phys 2009;36(5):1602–1609.
25. Fardon DF, Williams AL, Dohring EJ, Murtagh FR, Gabriel Rothman SL, Sze GK. Lumbar disc nomenclature: version 2.0: recommendations of the combined task forces of the North American Spine Society, the American Society of Spine Radiology and the American Society of Neuroradiology. Spine J 2014;14(11):2525–2545.
26. Pfirrmann CW, Dora C, Schmid MR, Zanetti M, Hodler J, Boos N. MR image-based grading of lumbar nerve root compromise due to disk herniation: reliability study with surgical correlation. Radiology 2004;230(2):583–588.
27. Genders TS, Spronk S, Stijnen T, Steyerberg EW, Lesaffre E, Hunink MG. Methods for calculating sensitivity and specificity of clustered data: a tutorial. Radiology 2012;265(3):910–916.
28. Johnson TR. Dual-energy CT: general principles. AJR Am J Roentgenol 2012;199(5 Suppl):S3–S8.
29. Wassenaar M, van Rijn RM, van Tulder MW, et al. Magnetic resonance imaging for diagnosing lumbar spinal pathology in adult patients with low back pain or sciatica: a diagnostic systematic review. Eur Spine J 2012;21(2):220–227.
30. Alsaleh K, Ho D, Rosas-Arellano MP, Stewart TC, Gurr KR, Bailey CS. Radiographic assessment of degenerative lumbar spinal stenosis: is MRI superior to CT? Eur Spine J 2017;26(2):362–367.